Technical Report
TR-23-17
September 2023

Evaluation of shoreline displacement and glacial erosion at Forsmark using in situ ^{14}C in quartz

Bradley W Goodfellow
Arjen P Stroeven
Alexander Lewerentz
Kristina Hippe
Jakob Heyman
Nathaniel A Lifton
Marc W Caffee

SVENSK KÄRNBRÄNSLEHANTERING AB

SWEDISH NUCLEAR FUEL
AND WASTE MANAGEMENT CO

Box 3091, SE-169 03 Solna
Phone +46 8 459 84 00
skb.se

SVENSK KÄRNBRÄNSLEHANTERING

ISSN 1404-0344
SKB TR-23-17
ID 2009124

September 2023

Evaluation of shoreline displacement and glacial erosion at Forsmark using in situ ^{14}C in quartz

Bradley W Goodfellow[1], Arjen P Stroeven[2,3], Alexander Lewerentz[1], Kristina Hippe[4], Jakob Heyman[5], Nathaniel A Lifton[6,7], Marc W Caffee[6,7]

1 Geological Survey of Sweden
2 Department of Physical Geography, Stockholm University
3 Bolin Centre for Climate Research, Stockholm University
4 Klimsa Kurt Gisbert Dr. Büro für Umweltplanung
5 Department of Earth Sciences, University of Gothenburg
6 Department of Earth, Atmospheric, and Planetary Sciences, Purdue University
7 Department of Physics, Purdue University

Keywords: Bedrock exposure dating, In situ ^{14}C, Forsmark, Glacial erosion, Postglacial isostatic uplift, RSL, Shoreline displacement curve.

Abstract

The aim of this study is to validate the Holocene relative sea-level (RSL) curve (or shoreline displacement curve) for Forsmark using ^{14}C produced in situ in quartz-bearing bedrock (in situ ^{14}C). Having an accurate representation of the Holocene RSL evolution at Forsmark is important for Svensk Kärnbränslehantering AB (SKB) from at least two aspects. In the safety assessments for the planned spent fuel repository and for the existing repository for short-lived radioactive waste (SFR), the RSL curve is used as input in models describing the landscape development in the Forsmark area. Also, the RSL is used to constrain model estimates of rates and depths of glacial erosion from inherited components of cosmogenic ^{10}Be and ^{26}Al produced in situ in quartz in bedrock surfaces.

The existing Holocene RSL curve used at SKB was developed prior to the Safety Repository (SR) site-assessment for the spent fuel repository and was based on ^{14}C dating of organic material from isolation basins. In subsequent Preliminary Safety Assessment Reports (PSAR) for the spent fuel repository and SFR, this curve was updated based on more recent data and empirical modelling. However, the updates resulted in only minor modifications of the original RSL curve, and it was therefore decided to keep the original curve also for the PSAR assessments. In this study, in situ ^{14}C is used to validate the updated RSL curve rather than the original one. However, given the minor differences between the curves, the conclusions drawn in this study apply to both.

An initial measurement of six in situ ^{14}C measurements was completed during 2018 to test the RSL. Four samples are all older than SKB's RSL curve and could form a consistent basis for an alternative RSL curve, if supported by additional samples along the elevation gradient. Two samples yield exposure ages younger than the RSL-based time of emergence, with the ^{14}C concentration of one of those being unexplainably low for its elevation. Because these six ages are non-systematic with respect to both elevation and SKB's RSL curve, we interpret the in situ ^{14}C data as being equivocal. To understand the reasons for this, we revisited the sampled sites and hypothesize that the measured concentrations of in situ ^{14}C may have been problematic because vein quartz or hydrothermally altered bedrock had been sampled. Quartz in both lithologies often contains fluid and vapour phase inclusions. Depending on their composition, these inclusions might complicate assessment of the in situ ^{14}C production rate and/or measurement of in situ ^{14}C concentrations.

The present study was initiated to address these problems and to test the existing RSL curve with ten new bedrock samples for in situ ^{14}C age determination, using a revised sampling strategy. Five samples are from bedrock outcrops within a region positioned below the highest post-glacial shoreline and occur along an elevation transect extending southwards from Forsmark. This dataset yields an independent chronology of landscape emergence, and thus can be used to validate SKB's existing RSL curve for Forsmark. An additional five samples are from bedrock outcrops 100 km to the west of Forsmark, above the highest post-glacial shoreline. The in situ ^{14}C concentrations in these latter samples should reflect a local deglaciation age and provide a valuable comparison dataset against which the samples located below the highest coastline in the vicinity of Forsmark can be evaluated. We complemented the sampling with thin section analyses to evaluate quartz quality and all samples underwent laboratory preparation and accelerator mass spectrometry at PRIME Lab, Purdue University, USA.

The ten new in situ ^{14}C measurements provide robust age constraints that compare favorably with the Forsmark RSL curve derived from ^{14}C dating of organic material in isolation basins and with the regional deglaciation chronology. They therefore supersede the initial in situ ^{14}C dataset, which we now exclude from further consideration. Previous interpretations of glacial erosion from ^{10}Be and ^{26}Al produced in situ in quartz therefore remain valid.

Sammanfattning

Syftet med denna studie är att utvärdera strandlinjeförskjutningsmodellen (RSL – relative sea-level curve) för Forsmark under holocen med hjälp av ^{14}C som producerats in situ i kvarts i berggrunden. En tillförlitlig RSL-modell för Forsmark är viktig av minst två anledningar. För säkerhetsanalyser för den planerade slutförvarsanläggningen för använt kärnbränsle (SFK) och för det befintliga slutförvaret för kortlivat radioaktivt avfall (SFR) har RSL-modellen använts för att beräkna landhöjningen i landskapsutvecklingsmodeller. Därutöver har RSL-modellen använts, tillsammans med kosmogen ^{10}Be och ^{26}Al in situ i kvarts från berggrundsytan, för att uppskatta hastighet och djup av glacial erosion.

Den etablerade RSL-modellen som används av Svensk Kärnbränslehantering AB (SKB) togs fram innan säkerhetsanalysen SR-site för SFK och baseras, i motsats till den metodik som använts i denna studie, på ^{14}C-åldersbestämningar av organiskt material från isolationsbassänger. I de efterföljande säkerhetsanalyserna PSAR för både SFK och SFR uppdaterades RSL-modellen med hjälp av nyare data och empirisk modellering. Dessa uppdateringar innebar dock bara små förändringar av den ursprungliga RSL-modellen, varför det trots allt beslöts att använda den ursprungliga modellen i PSAR. I denna studie används dock in situ ^{14}C för att utvärdera den uppdaterade RSL-modellen, men givet att skillnaderna mellan de två modellerna är väldigt små är slutsatserna från denna studie relevanta för dem båda. En serie av sex ^{14}C-mätningar utfördes 2018 för att utvärdera RSL-modellen. Av dessa gav en datapunkt en implicerad ålder som är avsevärt yngre än förväntat för provtagningslokalens höjd över havet, två datapunkter som skär RSL-modellen och tre datapunkter med indikerade åldrar som är äldre än förväntat. Eftersom det saknas samband mellan dessa åldrar och såväl höjd över havet som den ursprungliga RSL-modellen tolkar vi dessa ^{14}C data som tvivelaktiga. Provtagningslokalerna återbesöktes och därefter fastslogs att en möjlig orsak till detta är att kvartsådror och hydrotermalt omvandlade bergarter hade provtagits, vilket kan ha påverkat ^{14}C-analyserna. Kvarts från båda dessa geologiska material innehåller med hög sannolikhet vätskeinneslutningar som har negativ inverkan på provberedningen, vilket kan störa produktionstakten och/eller mätningen av in situ ^{14}C.

Den här studien initierades för att adressera tidigare tillkortakommanden och för att utvärdera den ursprungliga RSL-modellen. Tio nya prover insamlades för in situ ^{14}C-analys av kvarts, utifrån en omarbetad provtagningsstrategi. Fem av dessa prover togs från hällar i ett område beläget under den postglaciala högsta strandlinjen och ligger på en höjdtransekt som löper söderut från Forsmark. Från dessa data bör en fristående kronologi för landhöjningen erhållas, vilken direkt utvärderar RSL-modellen för Forsmark. Ytterligare fem prover insamlades från hällar 100 km väst om Forsmark, ovanför den postglaciala högsta strandlinjen. In situ ^{14}C-halter i dessa prover bör återspegla lokala deglaciationsåldrar, vilka är värdefulla som jämförelse och för utvärdering av de data som erhölls från provtagningslokaler belägna under högsta strandlinjen vid Forsmark. Efter provtagning gjordes tunnslip av samtliga prov för mikroskopering i syfte att identifiera och kvantifiera eventuella vätskeinneslutningar i kvarts, varefter provmaterialet skickades till PRIME Lab, Purdue University, USA, för provberedning och analys med accelerationsmasspektrometri.

De 10 nya in situ ^{14}C-analyserna ger robusta åldersbestämningar som är väl jämförbara med såväl tidigare ^{14}C-åldersbesätmningar av organiskt material i isolationsbassänger som med den regionala deglaciationskronologin. Dessa mätningar ersätter det tidigare in situ ^{14}C-datasetet. Tolkningar av glacial erosion utifrån in situ ^{10}Be och ^{26}Al kvarstår därmed enligt tidigare studier.

Contents

1 Introduction

1.1 Study aim and relevance for SKB

The aim of this study is to validate the Holocene relative sea-level (RSL) curve (or shoreline displacement curve) for Forsmark (Brydsten 2009, SKB 2020 Appendix D, SKB 2023a Appendix G) using ^{14}C produced in situ in quartz-bearing bedrock (in situ ^{14}C). Having an accurate representation of the Holocene RSL evolution at Forsmark is important for SKB from at least two aspects. In the safety assessments for the planned spent fuel repository and for the SFR, the RSL curve is used as input in models describing the landscape development in the Forsmark area (e.g. SKB 2020). Also, the RSL curve is used to constrain model estimates of rates and depths of glacial erosion from inherited components of cosmogenic ^{10}Be and ^{26}Al produced in situ in quartz in bedrock surfaces (Hall et al. 2019).

The existing Holocene RSL curve used at SKB was developed prior to the SR site-assessment for the spent fuel repository and was based on ^{14}C dating of organic material from isolation basins (Brydsten 2009). The curve was subsequently updated for the PSAR using more recent data and empirical modelling (SKB 2020 Appendix D, SKB 2023a Appendix G). However, the resulting updated curve was found to closely match the original one, and thus the original curve was kept for use in the safety assessments. In this study, comparisons are made against the updated RSL curve presented in SKB (SKB 2020 Appendix D, SKB 2023a Appendix G). Given the close match between the RSL curves, the choice of curve against which in situ ^{14}C data are compared is noncritical for the study conclusions. Furthermore, it is reasonable to assume that any landscape modelling at SKB in the future will implement the updated RSL curve rather than the original one, and thus testing the validity of the updated curve will be useful also for that purpose. All usages of the RSL curve in this document refer to SKB's updated RSL curve.

1.2 Background

The RSL curve used by SKB has been constructed from radiocarbon ages of basal organic sediments in isolation basins along elevation transects (Robertsson and Persson 1989, Risberg 1999, Bergström 2001, Hedenström and Risberg 2003, Berglund 2005). We have previously used this curve as a basis for comparison with ^{10}Be and ^{26}Al cosmogenic nuclide apparent exposure ages of bedrock outcrops along an elevation transect extending southwards from Forsmark (Hall et al. 2019). An 'apparent' exposure age is derived from a simple calculation from the nuclide concentration (Lal 1991, Gosse and Phillips 2001). However, correctly interpreting the exposure age relies on modelling that considers geological factors that can reduce the nuclide concentration relative to the time since initial subaerial exposure (such as erosion and burial by glacial ice, water, snow, and/or soil (Gosse and Phillips 2001, Schildgen et al. 2005, Ivy-Ochs and Kober 2008). The comparison with SKB's RSL curve can test the premise that concentrations of cosmogenic nuclides in exposed bedrock at Forsmark solely reflect the exposure duration since deglaciation and subsequent landscape emergence above sea level. Ages calculated from ^{10}Be and ^{26}Al would then mirror SKB's RSL curve for their corresponding elevations (but be slightly older because of nuclide production during landscape emergence through shallow water induced by isostatic rebound following the last glaciation). For this to work, the cosmogenic nuclide inventory from previous exposure periods (i.e., an inherited inventory), which is stored largely in the uppermost 3 m of bedrock (Gosse and Phillips 2001), needs to have been removed by glacial erosion during the last ice sheet phase (during Marine Isotope Stage 2; MIS2, 24–12 thousand years (ka) before present (BP)). However, this is not the case (Figure 1-1). Because most nuclide concentrations indicate accumulation over surface exposure durations that extend well beyond the Holocene, the implication is that for these sampled bedrock surfaces, erosion during the last glacial cycle was limited to < 3 m (thereby allowing for some of the nuclide accumulation during periods of subaerial exposure prior to the last glaciation to remain). For a subset of samples, there appears to be a systematic offset against the RSL curve. Whereas this too could be due to nuclide inheritance, differences were small enough to query whether they might in fact indicate that production of datable organic material in isolation basins did not begin immediately upon landscape emergence above sea level, but rather was delayed by environmental conditions. The implication of this potential delay would be an offset of the Holocene RSL curve used by SKB, because it would be based on age constraints that are too young.

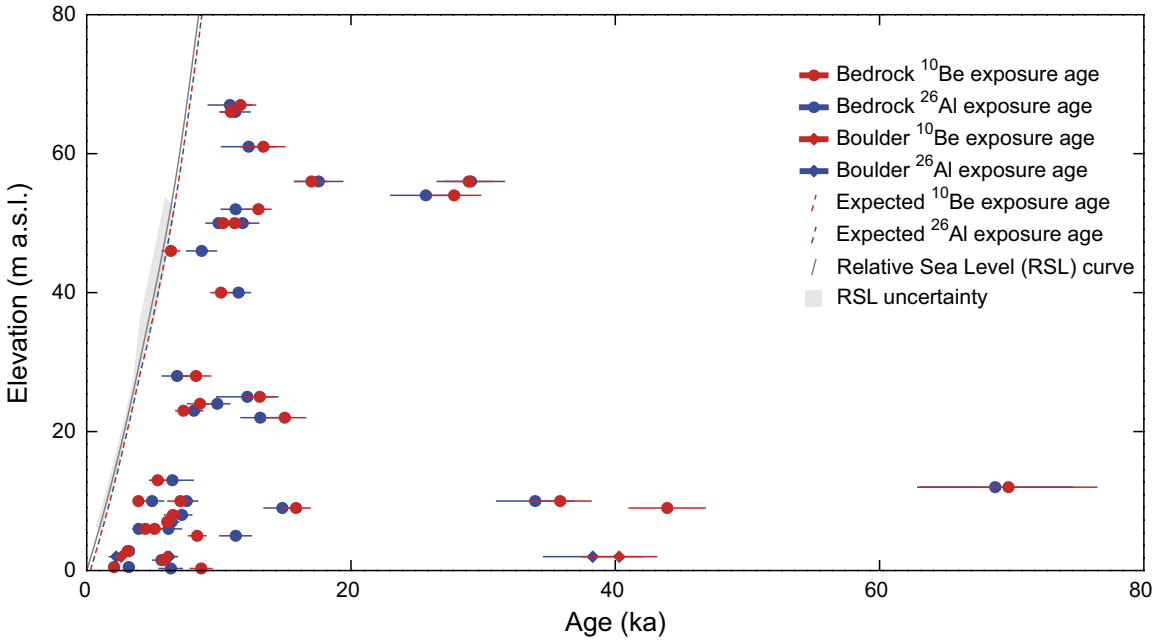

Figure 1-1. *Apparent ^{10}Be and ^{26}Al exposure ages, assuming a single period of full exposure to cosmic rays, plotted against sample elevation. Horizontal lines indicate external age uncertainty (1σ) for each sample. The grey line shows SKB's Holocene Relative Sea Level (RSL) curve for Forsmark and the red and blue dashed lines show expected ^{10}Be and ^{26}Al exposure age curves, respectively. These latter two curves account for subaqueous production of cosmogenic nuclides during isostatically driven landscape emergence through shallow water. The RSL curve is based on radiocarbon dating of isolation events (Robertsson and Persson 1989, Risberg 1999, Bergström 2001, Hedenström and Risberg 2003) and a shoreline displacement reconstruction by Påsse and Daniels (2015). Modified from Hall et al. (2019) with exposure age calculations done using the expage-202306 calculator. All three sampled boulders are located < 5 m a.s.l.*

To validate SKB's RSL curve, we applied a third cosmogenic nuclide, in situ ^{14}C, to six locations along the elevation transect during the Hall et al. (2019) glacial erosion study (Figure 1-2). We used in situ ^{14}C because it potentially circumvents an overt reliance on the need for deep erosion (> 3 m) to remove an inherited signal from previous exposure periods (Gosse and Phillips 2001). In addition, ^{14}C produced by muons will not accumulate to high levels because of rapid decay. Because of its short half-life of 5 700 ± 30 years, nuclide inheritance will have largely decayed away if ice sheet burial at these sites during MIS2 exceeded 25–30 ka, i.e., ca 5 half-lives (Briner et al. 2014).

Four samples (17-23, 16-04, 16-07, 16-20; Figure 1-2) from Hall et al. (2019) are all older than the RSL curve and could form a consistent basis for an alternative RSL curve, if supported by additional samples along the elevation gradient. Two samples (17-24 and 16-22) yield exposure ages younger than the RSL-based time of emergence, with the ^{14}C concentration of sample 16-22 being unexplainably low for its elevation. Because these six ages are non-systematic both with elevation and with respect to the RSL curve, we interpret the in situ ^{14}C data as being equivocal.

Kleman et al. (2020) have since identified ice-free conditions around Idre (NW, and therefore up-ice, of Forsmark) during MIS3 (ca 55–35 ka BP), which appears to imply inundation of Forsmark by ice after 35 ka BP. This result is consistent with ice sheet evolution at Forsmark in SKB's reconstruction of the last glacial cycle (SKB 2020, Figure 4-19). Combined with a well-constrained final deglaciation around 10.8 ka BP (Stroeven et al. 2016, SKB 2020), it appears that Forsmark has most recently been inundated by glacial ice for only 24 ka, or less. Consequently, in situ ^{14}C concentrations could reflect subaerial exposure of bedrock at Forsmark during MIS3 in addition to Holocene exposure following landscape emergence above sea level, resulting in an offset towards older ages relative to the RSL curve for Forsmark.

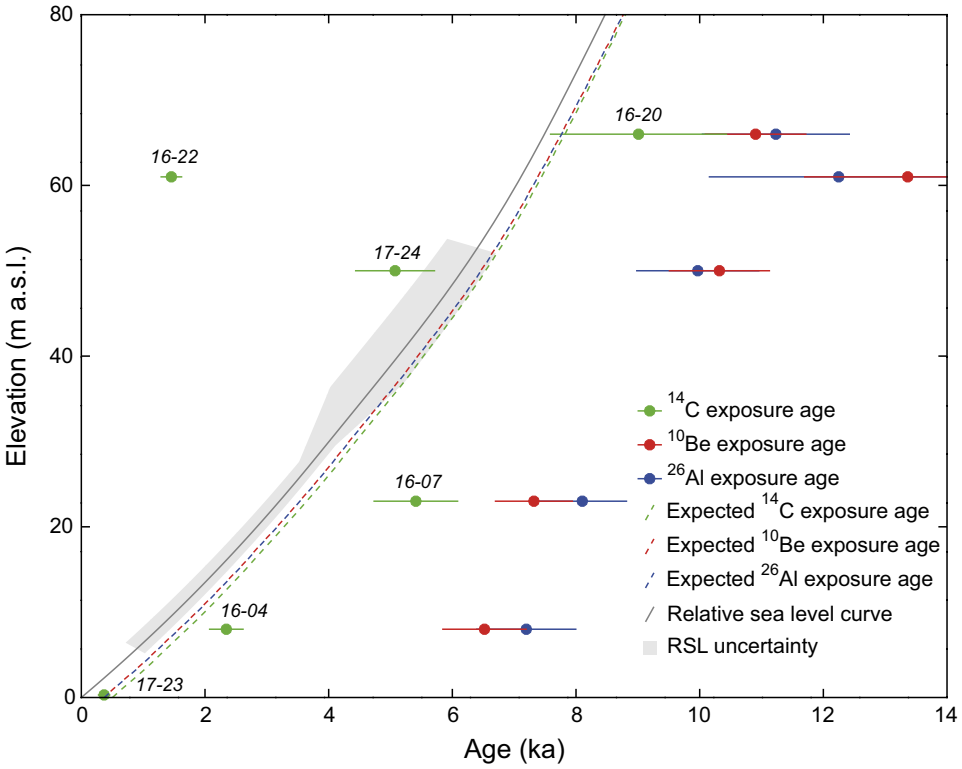

Figure 1-2. *Exposure ages from ^{10}Be, ^{26}Al (Hall et al. 2019), and unpublished ^{14}C concentrations in quartz for bedrock surfaces along an elevation gradient at Forsmark and adjacent Uppland. Ages are shown relative to the RSL curve established from radiocarbon dating and against expected age curves, which account for sub-aqueous production of cosmogenic nuclides as the landscape emerges through shallow water during isostatic uplift. Exposure age uncertainties are 1σ external. The RSL curve is from SKB (2020) and uncertainties for the 1–6 ka interval are calculated from the original radiocarbon data in Hedenström and Risberg (2003).*

To better understand these inconsistent in situ ^{14}C concentrations, we re-examined the six sample sites in 2020, and analyzed thin sections of the samples under an optical microscope (Goodfellow et al. 2020). A seventh site (16-23) was also assessed because its sample number had inadvertently been confused with 17-23. One sample was from metavolcanic rock that also hosted quartz veins (17-23), one was from fine-grained metavolcanic ash siltstone of rhyolitic–dacitic composition (16-23), two from quartz veins (16-07, 17-24), and one from hydrothermally altered volcanic rock (16-22; Goodfellow et al. 2020). These lithologies are either precipitated from or have been infiltrated by hydrothermal fluids and are therefore likely to host quartz fluid and vapour phase inclusions. Only two samples, 16-04 and 16-20, were taken from granitoid matrix. However, even these samples appear problematic because they yielded only ~20 g of clean quartz for ^{10}Be and ^{26}Al measurements (Hall et al. 2019). For some of these samples, the measurement of in situ ^{14}C may therefore have been compromised by inclusions in quartz.

Fluid and vapour phase inclusions in quartz were indeed confirmed on thin sections of the samples (Goodfellow et al. 2020). Subsequent Raman analyses of vapour phase inclusions confirmed the presence of N_2 in all six samples. The presence of N_2 in inclusions has the potential to be problematic because ^{14}C can be produced from absorption of thermal neutrons by ^{14}N (Kim et al. 2007, Dunai 2010, p. 46). This is the dominant method for production of atmospheric ^{14}C (from N_2) and potentially provides an additional production pathway not accounted for in our exposure age calculations. However, we cannot say definitively that this possible production mechanism is a significant influence on those measurements because we have no quantitative estimate of how much N_2 may be present in the samples. It is perhaps more likely that there could be procedural sources for the discrepancies because the age offsets of these six in situ ^{14}C measurements are neither systematically older nor younger than the RSL curve. Regardless of the exact cause, which we are still working to resolve, something clearly went wrong with this sample batch, to the extent that the data are challenging to interpret.

In addition to opening research into previously undocumented complications for in situ ^{14}C dating, this initial data set has two major implications for the current study. Firstly, if offsets from the RSL curve might be attributable either to characteristics inherent to quartz from different lithologies or to laboratory sources, then perhaps in situ ^{14}C inheritance is not an issue in testing the reliability of the existing RSL curve using in situ ^{14}C on bedrock. Secondly, if in situ ^{14}C yields vary with the source or history of the quartz, then avoiding the metamorphic or altered rock types initially targeted for sampling, might yield more reliable in situ ^{14}C concentrations reflective of the timing of post-glacial emergence above sea level. These implications motivate the present study, which includes resampling locations previously studied (Hall et al. 2019) but avoiding hydrothermally altered quartz.

1.3 Hypotheses and sampling rationale

Sampling of bedrock outcrops above and below the highest (post-glacial) shoreline for in situ ^{14}C informs the timing of Holocene emergence of the Forsmark landscape above sea level. The rationale for this is as follows. Firstly, samples above the highest shoreline should unequivocally yield deglaciation ages in parity with the Fennoscandian deglaciation chronology (Stroeven et al. 2016) for sampled locations. Demonstrating this would reinforce both the accuracy of the deglaciation chronology (and therefore of the local estimate of deglaciation at Forsmark from the chronology) and that the revised cosmogenic nuclide sampling strategy yields high purity quartz. Secondly, samples below the highest shoreline would only deviate from the expected deglaciation age of 10.8 (± 0.1–0.5) ka BP for a time equivalent to their post-glacial duration below sea level and should thus reliably establish a shoreline emergence curve. Samples below the highest shoreline are taken from a NE to SW elevation transect from the low-elevation Forsmark-Uppland region, whereas samples above the highest shoreline are located further west, in Dalarna and Gävleborg (Figure 1-3).

Comparing concentrations of in situ ^{14}C in bedrock located above and below the highest shoreline permits a test of the following three working hypotheses:

(i) Our initial batch of in situ ^{14}C samples yielded generally erroneous results. A key indication that these data include erroneous in situ ^{14}C concentrations is the presence of two outliers, which yield apparent exposure ages younger than the RSL curve (Figure 1-2). In contrast, systematic increases in age with increasing elevation are observed both in organic radiocarbon derived from basal sediments of isolation basins at different elevations (i.e., RSL curve) and in ^{10}Be and ^{26}Al in bedrock (Figure 1-2). A further indication of erroneous data is that none of the six in situ ^{14}C data points falls on the RSL curve, which is constructed using well-established organic radiocarbon dating. If new measurements of in situ ^{14}C indicate ages that are consistently older with increasing elevation, then it is possible to identify inconsistent data in our initial batch.

(ii) The existing RSL curve accurately reflects the timing of landscape emergence. Demonstrating this would require, firstly, that new in situ ^{14}C measurements plot, within uncertainty, on the RSL curve. Secondly, it would require that in situ ^{14}C concentrations from above the highest shoreline are consistent, both internally and with the regional last deglaciation chronology (Stroeven et al. 2016). If so, we can infer that the new in situ ^{14}C samples, including those located below the highest shoreline, lack inheritance from MIS3.

(iii) Cosmogenic nuclide production rates of ^{14}C, ^{10}Be, and ^{26}Al are underestimated for east-central Sweden. It is difficult to envisage that the local production rates for all three nuclides are incorrect. However, if the new in situ ^{14}C concentrations from above and below the highest shoreline display an offset from the latest deglaciation chronology by Stroeven et al. (2016) and the RSL curve, respectively, and if the latter are consistent with equivalent ^{10}Be and ^{26}Al data, then we need to further evaluate this possibility. This is because the current RSL curve and regional deglaciation chronology are well-established, and it is unlikely that emergence of the Forsmark landscape above sea level occurred centuries to thousands of years (inferred from the cosmogenic nuclide concentrations in Figure 1-2) earlier than indicated by the RSL curve.

Testing these hypotheses ultimately allows us to evaluate the reliability of RSL curves constructed from organic radiocarbon dating, which are often used in geodynamic modelling. The ubiquitous presence of bedrock in formerly glaciated coastal settings (e.g. Kleman et al. 2008), which is also frequently quartz-bearing, also allows us to present a complementary methodology to the construction of RSL

curves. Testing of established RSL curves also ultimately strengthens interpretations of rates and depths of glacial erosion from nuclide ^{10}Be and ^{26}Al inheritance in landscapes, such as Forsmark, that have undergone post-glacial emergence above sea level (cf Hall et al. 2019).

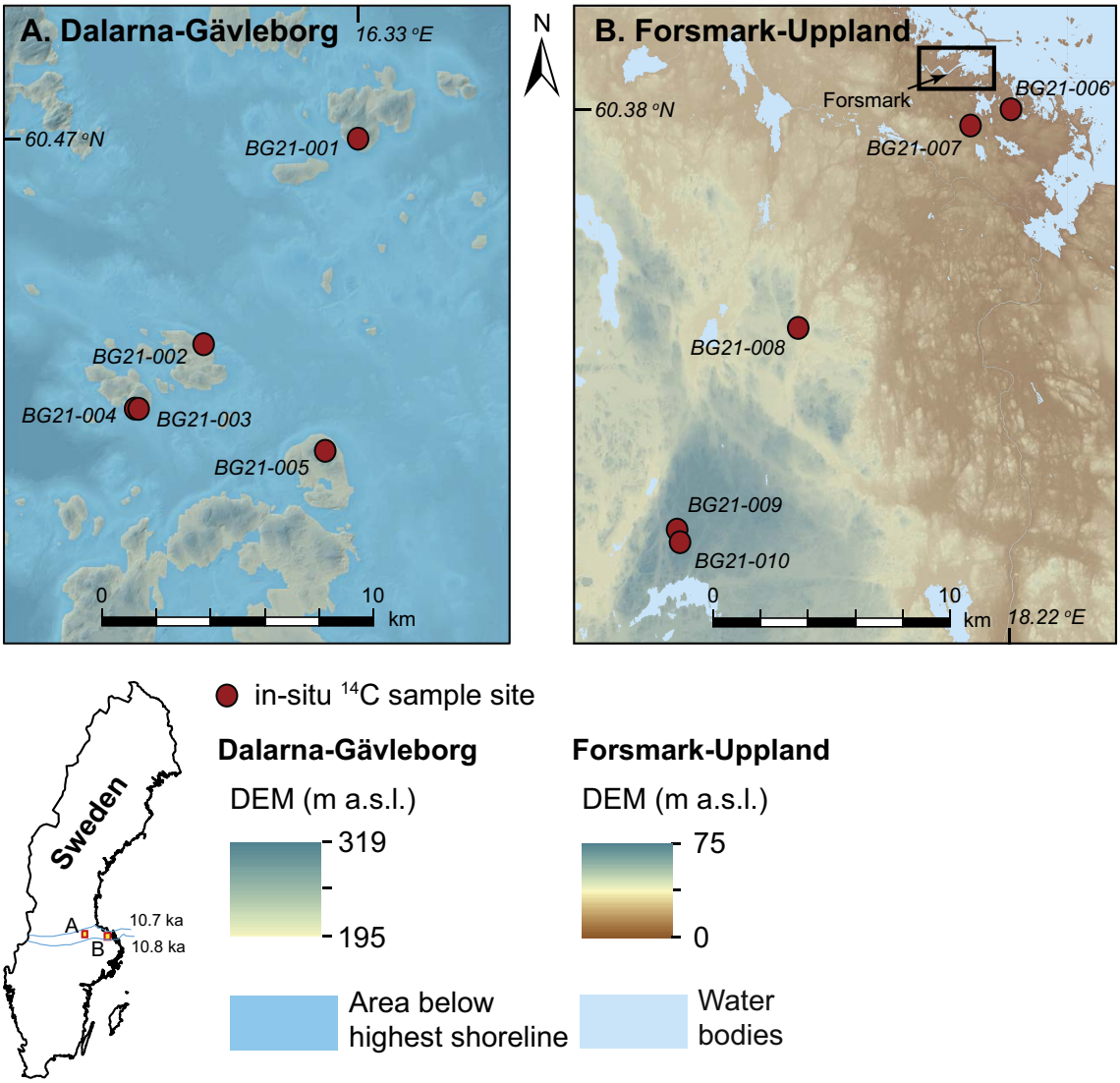

Figure 1-3. *Sample locations for in situ ^{14}C dating in A) Dalarna-Gävleborg and B) Forsmark-Uppland. The five Dalarna-Gävleborg sample sites are located above the highest shoreline (shown), whereas the five sample sites from Forsmark-Uppland are located below the highest shoreline (not shown because the entire area was submerged). See inset for locations of panels A and B and for the 10.7 ka BP and 10.8 ka BP retreat isochrones from Stroeven et al. (2016). The rectangle in panel B indicates the location of SKB's existing and planned facilities at Forsmark.*

2 Methods

2.1 Sampling of bedrock outcrops for in situ ^{14}C measurement

To explore how in situ ^{14}C concentrations in bedrock reflect the post-glacial timing of emergence of the Forsmark landscape above sea level and subsequent inferences of this for long-term, ≤ 1 Ma, patterns of glacial erosion from ^{10}Be and ^{26}Al inheritance, we use the following strategy for sampling quartz:

(i) A rigorous scheme was applied to minimise the possibility of sampling quartz altered through hydrothermal processes. This meant that we avoided major pegmatite intrusions, outcrops located in major deformation zones, outcrop-scale veins, fractures, and adjacent rock volumes. Consequently, sampling was done on outcrops of metagranitoid from the early-Svecokarelian GDG-GSDG suite that dominates the Bergslagen lithotectonic unit (Stephens and Jansson 2020).

(ii) A petrological examination using transmitted light polarization microscopy was applied to thin sections to ascertain that the quartz was unlikely to contain multi-fluid phase, vapour phase, or solid-phase inclusions.

(iii) We collected five samples for in situ ^{14}C dating along a SW–NE transect near Forsmark (Figure 1-3b). These outcrops were chosen because they span an elevation gradient of 9.4–56.0 m a.s.l. and can therefore be diagnostic for validating the existing RSL curve. Four of these samples were taken from granitic outcrops that host sites we previously sampled for ^{10}Be and ^{26}Al, thus offering a pathway to evaluate nuclide inheritance in our ^{10}Be and ^{26}Al data (Hall et al. 2019).

(iv) We collected five samples of granitic bedrock for in situ ^{14}C analyses from locations above the well-constrained highest shoreline (located ~195 m a.s.l., ~100 km west of Forsmark; Figure 1-3a) to determine the age of local deglaciation. According to the deglaciation chronology of Stroeven et al. (2016), the samples should return in situ ^{14}C apparent exposure ages of 10.8 (± 0.1–0.5) ka BP (Figure 1-3).

(v) Sample locations were logged on a 2 m-resolution LiDAR digital elevation model (DEM) displayed in ArcGIS 10 on a tablet computer. A GPS add-in tool in ArcGIS 10 was used to record positional data, within a horizontal precision of 2 m. The elevation of each sample location was extracted from the DEM and has a precision of tens of centimetres. The influence of these minor positional uncertainties on our ^{14}C calculations is trivial and none of the sample sites is influenced by topographic shielding that could reduce the accumulation of ^{14}C in bedrock.

(vi) All samples were collected from bedrock using an angle grinder, which permits sampling of hard bedrock isolated from outcrop edges, fractures, and quartz veins, and consistently limits sample thicknesses to 3 cm.

(vii) Each sampled bedrock outcrop formed a local topographic high, which minimizes the risk of burial by soil and minimizes snow accumulation. Moss mats were present on all sampled outcrops. Although we avoided sampling bedrock that was moss-covered, we cannot be certain that moss mats did not formerly cover the sample sites. Given a compressed thickness of 0.5 cm and an estimated density of 0.7 g/cm^3, this may have contributed to a shielding of the sampled rock surfaces of 0.35 g/cm^2, which is negligible and is therefore excluded from our age inferences.

2.2 Laboratory preparation for accelerator mass spectrometry (AMS)

Samples were physically and chemically processed at the Purdue Rare Isotope Measurement Laboratory (PRIME Lab) at Purdue University, U.S.A. Concentrations of in situ ^{14}C were determined from purified quartz separates through automated procedures (Lifton et al. 2023). Approximately 5 g of quartz from each sample was added to a degassed $LiBO_2$ flux in a re-usable 90 % Pt/10 % Rh sample boat and heated to 500 °C for one hour in ca 6.7 kPa of Research Purity O_2 to remove atmospheric contaminants, which were discarded. The sample was then heated to 1 100 °C for three hours to dissolve the quartz and release the in situ ^{14}C, again in an atmosphere of ca 6.7 kPa of Research Purity O_2 to oxidize any evolved carbon species to CO_2. The CO_2 from the 1 100 °C step was then purified, measured quantitatively, and

converted to graphite for ^{14}C AMS measurement at PRIME Lab (Lifton et al. 2023). To test for data reproducibility, sample BG21-002 was randomly selected to undergo laboratory preparation and AMS a second time. Measured concentrations of in situ ^{14}C are calculated from the measured isotope ratios via accelerator mass spectrometry following Hippe and Lifton (2014).

2.3 Exposure age calculations

The expage calculator version 202303 (http://expage.github.io/calculator) is used to calculate apparent exposure ages. It is based on the original CRONUS calculator v. 2 (Balco et al. 2008), the LSD production rate scaling (Lifton et al. 2014), and the CRONUScalc calculator (Marrero et al. 2016), using the geomagnetic framework of Lifton (2016) with the SHA.DIF.14k model for the last 14 ka. Exposure ages are calculated using resulting time-varying ^{14}C production rates accounting for decay and interpolated to match the measured ^{14}C concentration. The production rate from muons is calibrated against the Leymon High core ^{14}C data of Lupker et al. (2015) and the production rate from spallation is calibrated against updated global ^{14}C production rate calibration data (Schimmelpfennig et al. 2012, Young et al. 2014, Lifton et al. 2015, Borchers et al. 2016, Phillips et al. 2016, Koester and Lifton 2023). This calibration is done iteratively for spallation and muons to reach convergence, using the expage production rate calibration methods (Figure 2-1). Exposure age calculations along the Forsmark-Uppland transect account for ^{14}C production during emergence through shallow water. However, burial of sampled surfaces by snow is excluded from the age calculations for all sample sites because we know neither how snow burial depths and durations vary between sites nor through the Holocene. The effect of snow burial would be to slightly decrease cosmogenic nuclide production in the underlying rock surface (Schildgen et al. 2005) and we have minimized this effect through our sampling strategy.

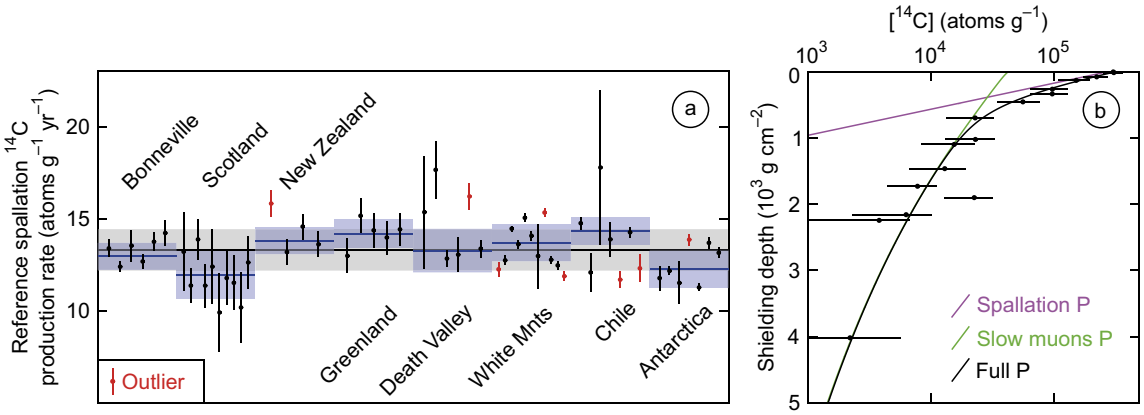

Figure 2-1. *Production rate calibration of ^{14}C in quartz. (a) Reference spallation ^{14}C production rate calibration based on data from Schimmelpfennig et al. (2012), Lifton et al. (2015), Borchers et al. (2016), Phillips et al. (2016), and Young et al. (2014), corrected per Hippe and Lifton (2014) and compiled in Koester and Lifton (2023). An uncertainty-weighted production rate is calculated for each of the eight sites (blue). Outliers, which are not included in the uncertainty-weighted production rates, are determined based on the requirement that there should be at least three samples yielding a reduced chi-square statistic (X^2_R) with a P-value of at least 0.05 for the assumption that the individual production rates from a site are derived from one normal distribution. For X^2_R, but not the uncertainty-weighting, we use the largest of the sample-specific production rate uncertainty based on the ^{14}C concentration uncertainties and 5 % of the sample production rate. This procedure does not punish samples with low measurement uncertainties, which otherwise risk exclusion as outliers. We adopt a global reference spallation ^{14}C production rate of 13.30 ± 1.13 atoms g^{-1} yr^{-1}, calculated as the arithmetic mean of the eight site production rates with the uncertainty being based on the standard deviation of all included single sample production rates, excluding outliers. (b) Calibration of ^{14}C production rate from muons based on the data of Lupker et al. (2015). The calibration is based on the method used in the CRONUScalc calculator (Marrero et al. 2016, Phillips et al. 2016). The figure shows the best fit ^{14}C concentration profiles produced from spallation, slow muons, and full production. The best fit yields near zero production from fast muons (cf Lupker et al. 2015). The production rate calibration has been carried out using the expage-202306 calculator in an iterative way to make the global reference spallation ^{14}C production rate converge with the production rate from muons.*

3 Results

Microscopic examination of a thin section from each of the ten samples revealed a varying degree of grain boundary migration, sub-grain division, and grain stretching, which are all indicative of metamorphic recrystallisation and deformation, as expected for metamorphosed granitoids. Fluid inclusions in quartz are observed for all samples, varying in abundance from minor to extensive (SKB 2023b). They occur as trails, following internal structures in the quartz crystals, and as a random scatter throughout the crystals. With rare exceptions only a single fluid phase is observed within the inclusions, which may cautiously be interpreted as indicative of a water-dominated composition. These characteristics exclude the presence of fluid inclusions interpreted as potentially problematic for measurement of in situ ^{14}C concentrations.

Inferred ages for the five in situ ^{14}C samples from the Forsmark-Uppland transect (below the highest shoreline) are shown relative to the existing Holocene RSL curve for Forsmark and the expected in situ ^{14}C exposure age curve considering subaqueous cosmogenic nuclide production (Figure 3-1; Tables 3-1 and 3-2). Exposure age uncertainties are large with internal uncertainties (measurement uncertainties; Balco et al. 2008) of 5–9 % and external uncertainties of 12–20 % (also including production rate uncertainties, which are high relative to ^{10}Be and ^{26}Al). Apparent exposure ages increase consistently with elevation and match expected ages within uncertainty, except for sample BG21-006, which has a simple exposure age 0.4 ka younger than expected. The two highest samples have near-identical apparent exposure ages and elevations. However, these samples provide independent ages because they are horizontally separated by 624 m (Figure 1-3b). There is now good agreement between ages inferred from these new in situ ^{14}C data and the existing RSL curve constructed from organic radiocarbon dating.

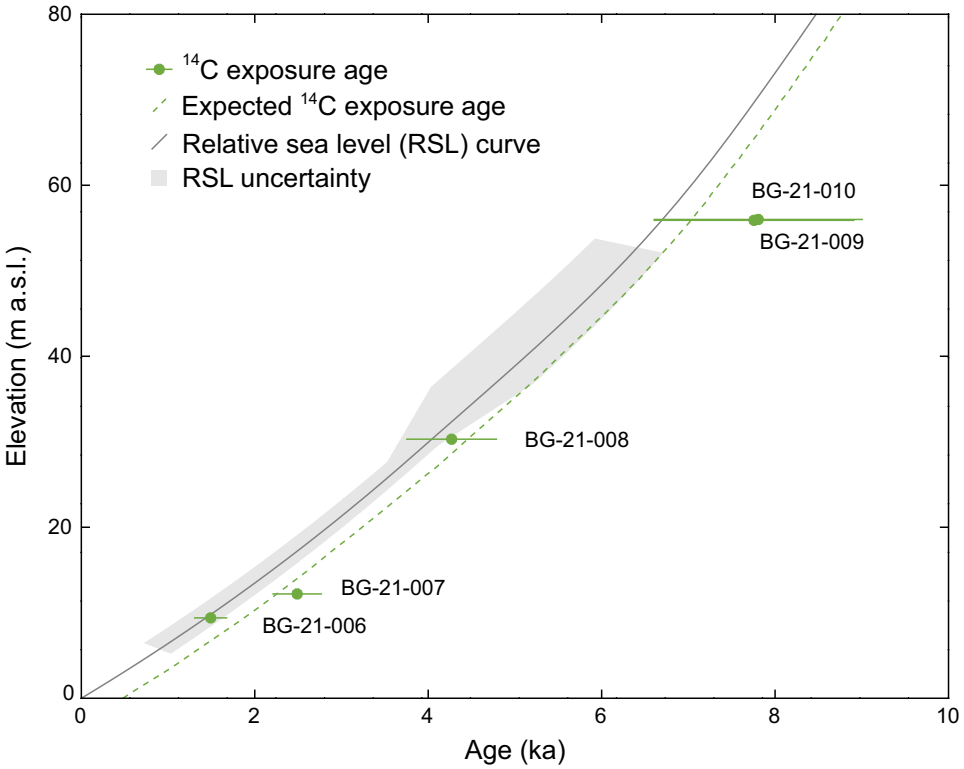

Figure 3-1. *Apparent ^{14}C exposure ages for five Forsmark samples from below the highest shoreline (Figure 1-3b; Table 3-1) with 1σ external uncertainties. The expected exposure ages are calculated assuming the RSL curve is correct, the ^{14}C spallation production rate is correct, partial exposure as the sample approaches the water surface, and full post-glacial exposure for the duration above sea level. Hence, the expected exposure age curve is a few hundred years older than the RSL curve. The RSL curve is from SKB (2020) and uncertainties for the 1–6 ka interval are calculated from the original radiocarbon data in Hedenström and Risberg (2003).*

Apparent exposure ages for the five in situ ^{14}C samples located above the highest shoreline in Dalarna and Gävleborg (Figure 1-3a) are shown in Figure 3-2 and Table 3-1. The weighted mean age from all five samples is 11.2 ± 1.3 ka BP. These data display a X_R^2 of 1.78 and a p-value of 0.13 based on 1σ internal uncertainties (Figure 3-2a), which does not support a rejection of the null hypothesis that the apparent exposure ages represent the same population. In addition to the samples being from the same population, the exposure ages are consistent, within uncertainty, with the expected deglaciation age of 10.8 (± 0.1–0.5) ka BP (Stroeven et al. 2016). Replicate measurements on sample BG21-002 closely agree and their weighted mean age is shown in Figure 3-2. Sample BG21-001 provides the youngest inferred age but, because this sample was from a low-profile outcrop (Figure 1-3a; SKB 2023b), this age may reflect partial shielding of the sampled bedrock surface by a past shallow soil cover or perhaps a deeper snow cover than the other sites. We therefore consider this sample as least likely to provide a reliable age. Removing this sample from consideration indicates that the remaining four sample sites are more clustered, with an older weighted mean age of 11.6 ± 1.1 ka BP, which displays a X_R^2 of 0.43 and a p-value of 0.73 based on 1σ internal uncertainties (Figure 3-2b).

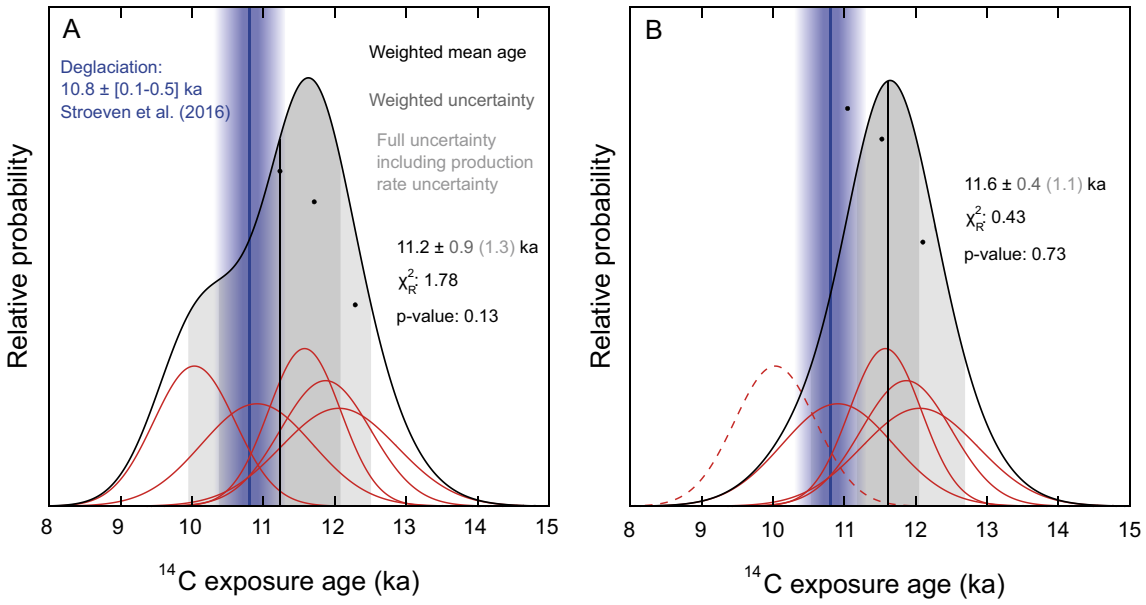

Figure 3-2. *Probability density plots of the exposure ages from samples above the highest shoreline (Figure 1-3a; Table 3-1). The individual samples (red curves) display 1σ internal uncertainty (measurement uncertainty). For the repeat sample BG21-002, the exposure age is calculated with a weighted mean ^{14}C concentration using a 2 % uncertainty. A. The probability density and data for all five samples. For the full set of samples, the cosmogenic nuclide ages yield a reduced chi-square (X_R^2) of 1.78 and a p-value of 0.13 based on internal uncertainties, which indicates that they are from the same population. B. The probability density and data with sample BG21-001 excluded as an outlier. These cosmogenic nuclide ages yield a X_R^2 of 0.43 and a p-value of 0.73 based on internal uncertainties, which again indicates that they are from the same population. All ages are referenced to the sampling year 2021. The weighted ages of 11.2 ± 1.3 ka BP and 11.6 ± 1.1 ka BP both overlap with the deglaciation age from Stroeven et al. (2016).*

Table 3-1. Extraction and measurement of in situ ^{14}C at PRIME Lab.

Sample ID	PCEGS #[a]	PLID[b]	Mass Quartz *(g)*	C yield *(ug)*	Diluted mass C *(ug)*	AMS Split Mass C *(ug)*	$\delta^{13}C$[c] *(‰$_{VPDB}$)*	$^{14}C/^{13}C$ *(10^{-11})*	$^{14}C/C_{total}$ *(10^{-13})*	^{14}C *(10^{6} at)*	[^{14}C] *(10^{5} at g^{-1})*[d]
BG21-001	146	202101960	5.02378	5.0 ± 0.1	393.8 ± 4.8	382.3 ± 4.6	−45.9 ± 0.2	0.3399 ± 0.0075	0.3412 ± 0.0079	0.6177 ± 0.0179	1.2296 ± 0.0357
BG21-002	147	202101961	5.02383	7.8 ± 0.1	303.3 ± 3.7	294.4 ± 3.6	−44.8 ± 0.2	0.4555 ± 0.0096	0.4623 ± 0.0102	0.6470 ± 0.0181	1.2879 ± 0.0360
BG21-003	148	202101962	5.0107	17.6 ± 0.3	303.4 ± 3.7	294.5 ± 3.6	−43.9 ± 0.2	0.4633 ± 0.0108	0.4709 ± 0.0113	0.6604 ± 0.0197	1.3180 ± 0.0393
BG21-002R	150	202201473	5.04116	7.7 ± 0.1	305.3 ± 3.7	296.4 ± 3.6	−45.2 ± 0.2	0.4558 ± 0.0135	0.4624 ± 0.0142	0.6519 ± 0.0237	1.2931 ± 0.0470
BG21-004	152	202101963	5.05927	11.9 ± 0.2	305.7 ± 3.7	296.8 ± 3.6	−44.6 ± 0.2	0.4618 ± 0.0079	0.4691 ± 0.0083	0.6630 ± 0.0159	1.3105 ± 0.0314
BG21-005	153	202101964	5.07578	4.6 ± 0.1	304.5 ± 3.7	295.6 ± 3.6	−45.4 ± 0.2	0.4600 ± 0.0127	0.4667 ± 0.0134	0.6566 ± 0.0225	1.2935 ± 0.0444
BG21-006	155	202101965	5.06572	5.5 ± 0.1	306.8 ± 3.7	297.8 ± 3.6	−45.2 ± 0.2	0.1277 ± 0.0056	0.1172 ± 0.0059	0.1243 ± 0.0101	0.2453 ± 0.0199
BG21-007	157	202101966	5.03589	6.9 ± 0.1	309.2 ± 3.8	300.1 ± 3.7	−45.0 ± 0.2	0.1684 ± 0.0051	0.1601 ± 0.0054	0.1922 ± 0.0096	0.3817 ± 0.0191
BG21-008	158	202101967	5.07653	4.0 ± 0.1	308.9 ± 3.8	299.9 ± 3.6	−45.4 ± 0.2	0.2357 ± 0.0063	0.2308 ± 0.0067	0.3015 ± 0.0119	0.5938 ± 0.0234
BG21-009	160	202101968	5.01906	55.3 ± 0.7	305.6 ± 3.7	296.6 ± 3.6	−38.0 ± 0.2	0.3339 ± 0.0095	0.3368 ± 0.0101	0.4601 ± 0.0170	0.9168 ± 0.0339
BG21-010	161	202101969	4.99961	42.2 ± 0.6	306.0 ± 3.7	297.0 ± 3.6	−40.1 ± 0.2	0.3320 ± 0.0068	0.3340 ± 0.0072	0.4565 ± 0.0132	0.9130 ± 0.0264

[a] PCEGS # = sample number in the Purdue Carbon Extraction and Graphitization System.

[b] PLID = PRIME Lab ID.

[c] Measurement uncertainty of ± 0.2 ‰$_{VPDB}$ (where VPDB is Vienna Peedee Belemnite).

[d] Corrected for procedural blank of (5.5952 ± 0.3713) × 10^4 atoms.

Table 3-2. In situ cosmogenic ^{14}C from quartz, Dalarna-Gävleborg and Forsmark-Uppland.

Sample ID	Lat (°)	Long (°)	Elevation (m a.s.l.)	Thickness (cm)	Density (g/cm^3)	Shielding factor	Erosion (cm/yr)	^{14}C ± 1σ (10^2 atoms/g)	^{14}C Age ± Unc.$^{Ext.}$ (± Unc.$^{Int.}$)[a] (ka BP)
BG21-001	60.47432	16.33134	236.5	3	2.7	1	0	1230 ± 36	9.9 ± 1.7 (± 0.6)
BG21-002	60.40615	16.22197	212.6	3	2.7	1	0	1288 ± 36	11.4 ± 2.2 (± 0.7)
BG21-002R	60.40615	16.22197	212.6	3	2.7	1	0	1293 ± 47	11.5 ± 2.3 (± 0.9)
BG21-003	60.38459	16.17649	216.3	3	2.7	1	0	1318 ± 39	11.9 ± 2.4 (± 0.8)
BG21-004	60.38451	16.17440	217.8	3	2.7	1	0	1311 ± 31	11.8 ± 2.3 (± 0.6)
BG21-005	60.36888	16.30526	248.1	3	2.7	1	0	1294 ± 44	10.8 ± 2.0 (± 0.8)
BG21-006	60.38490	18.22308	9.4	3	2.7	1	0	245 ± 20	1.5 ± 0.2 (± 0.1)
BG21-007	60.37892	18.19129	12.2	3	2.7	1	0	382 ± 19	2.5 ± 0.3 (± 0.1)
BG21-008	60.30504	18.04993	30.3	3	2.7	1	0	594 ± 23	4.3 ± 0.5 (± 0.2)
BG21-009	60.22988	17.94989	56.0	3	2.7	1	0	917 ± 34	7.8 ± 1.2 (± 0.5)
BG21-010	60.22431	17.95051	55.9	3	2.7	1	0	913 ± 26	7.8 ± 1.2 (± 0.4)

[a] Unc.$^{Ext.}$ is external uncertainty and Unc.$^{Int.}$ is internal uncertainty. Both are 1σ.

4 Discussion

Except for the lowest-elevation sample, our new data from the Forsmark-Uppland transect (i.e., below the highest shoreline) overlap, within uncertainty, the expected exposure age curve (Figure 3-1). This result indicates that our initial in situ ^{14}C data set (Figure 1-2), in which there was no overlap with the RSL curve within uncertainty, was unreliable. Hypothesis 1 is thereby supported (our initial batch of in situ ^{14}C data yielded generally erroneous results). Further inferences from the Forsmark-Uppland in situ ^{14}C data are that the construction of the existing RSL curve through organic radiocarbon dating is robust because it does not significantly underestimate the timing of landscape emergence, in support of hypothesis 2 (the existing RSL curve accurately reflects the timing of landscape emergence). Because these data conform with the existing RSL curve and because ages inferred from our in situ ^{14}C concentrations from above the highest shoreline conform with the expected deglaciation age (Figures 3-1 and 3-2), we can also exclude inheritance of in situ ^{14}C from a MIS3 interstadial. The data from above the highest shoreline further strengthens support for hypothesis 2 and rejects hypothesis 3 (cosmogenic nuclide production rates of ^{14}C, ^{10}Be, and ^{26}Al are underestimated for central-eastern Sweden). The latter is rejected with the caveat that the production rate of in situ ^{14}C in quartz requires further calibration to reduce uncertainties, preferably from local (Swedish) sites.

A key implication of these in situ ^{14}C data is that our inferences of past (and future) glacial erosion depths and rates from concentrations of ^{10}Be and ^{26}Al produced in situ in quartz (Hall et al. 2019) are essentially correct. This is because such inferences, based on ^{10}Be and ^{26}Al inheritance, rely on an accurate knowledge of the local timing of deglaciation. For most of the samples that yield an erosion rate solution for both ^{10}Be and ^{26}Al, glacial erosion was restricted to 0.04–0.09 m/ka or 0.4–1.1 m per ice cover period (Hall et al. 2019). Over the last 100 ka, this translates into a total erosion depth of only 1.6–3.5 m (Hall et al. 2019). Indeed, our new in situ ^{14}C data strengthens the interpretation in Hall et al. (2019) that projected total erosion is less than 1 m for the coming 100 ka and ranges from 5 to 28 m (25th–75th percentiles) for the coming 1 Myr.

The construction of RSL curves from organic radiocarbon dating is confirmed as being robust by our new in situ ^{14}C data. This motivates excluding the initial in situ ^{14}C data from further consideration. In contrast, we place high confidence in our new in situ ^{14}C data because: (i) inferred ages in samples from below the highest shoreline consistently increase with elevation and generally agree with the expected ages, within 1σ external uncertainty, assuming subaqueous cosmogenic nuclide production determined by the SKB (2020) RSL curve and full subaerial cosmogenic nuclide production (Figure 3-1). (ii) The five samples from above the highest shoreline are well-clustered and the weighted mean age (and full uncertainty) of 11.2 ± 1.3 ka BP overlaps with the expected deglaciation age of 10.8 (± 0.1–0.5) ka BP (Figure 3-2a). Removing the youngest age from consideration results in more strongly clustered ages (Figure 3-2b) and an older mean weighted age of 11.6 ± 1.1 ka BP, which still overlaps the expected deglaciation age within uncertainty. We therefore do not further discriminate between these results.

Our in situ ^{14}C data from above the highest shoreline highlight good potential for this nuclide to help constrain the deglaciation chronology of the Fennoscandian ice sheet for areas above the highest shoreline, especially inside its Younger Dryas margin, which is outlined by an almost continuous moraine belt (Lundqvist 1990, Andersen et al. 1995a, 1995b). The deglaciation of the Forsmark area, below the highest shoreline, is well constrained by clay-varve chronology (Strömberg 1989), but elsewhere there are vast areas where the post-Younger Dryas deglaciation remains poorly constrained by data (Stroeven et al. 2016). The potential for in situ ^{14}C measurements to fill in these data gaps helps to further motivate a local calibration of the in situ ^{14}C production rate. A Bayesian approach (e.g. Small et al. 2017) offers potential for further refinements to the age determinations of both shoreline displacement and deglaciation using in situ ^{14}C. Because of its short half-life and an improved sampling methodology, in situ ^{14}C may now be a prime candidate nuclide to date the last deglaciation also from boulders deposited along glacial flowlines; a technique practiced successfully using ^{10}Be (Stroeven et al. 2016, Margold et al. 2019, Norris et al. 2022).

5 Conclusions

Ten new in situ ^{14}C measurements on bedrock are consistent with the Forsmark RSL curve derived from organic radiocarbon dating of basal sediments in isolation basins (with one exception) and the Fennoscandian Ice Sheet deglaciation chronology from Stroeven et al. (2016). Results from this new independent method therefore verifies the RSL curve used in SKB safety assessments. Furthermore, the new measurements replace an initial set of six inconsistent in situ ^{14}C measurements, which we now exclude from further consideration. Interpretations of glacial erosion from ^{10}Be and ^{26}Al produced in situ in quartz therefore remain as stated in Hall et al. (2019). This study introduces the use of in situ ^{14}C in Fennoscandian Ice Sheet paleoglaciology and outlines a promise of its use as a basis for supporting future shoreline displacement studies and for tracking the deglaciation in areas that lack datable organic material, typically in locations above the highest shoreline.

6 References

SKB's (Svensk Kärnbränslehantering AB) publications can be found at www.skb.com/publications. SKBdoc documents will be submitted upon request to document@skb.se.

Andersen B G, Lundqvist J, Saarnisto M, 1995a. The Younger Dryas margin of the Scandinavian ice sheet – an introduction. Quaternary International 28, 145–146.

Andersen B G, Mangerud J, Sørensen R, Reite A, Sveian H, Thoresen M, Bergström B, 1995b. Younger Dryas ice-marginal deposits in Norway. Quaternary International 28, 147–169.

Balco G, Stone J O, Lifton N A, Dunai T J, 2008. A complete and easily accessible means of calculating surface exposure ages or erosion rates from ^{10}Be and ^{26}Al measurements. Quaternary Geochronology 3, 174–195.

Berglund M, 2005. The Holocene shore displacement of Gästrikland, eastern Sweden: a contribution to the knowledge of Scandinavian glacio-isostatic uplift. Journal of Quaternary Science 20, 519–531.

Bergström E, 2001. Late Holocene distribution of lake sediment and peat in NE Uppland, Sweden. SKB R-01-12, Svensk Kärnbränslehantering AB.

Borchers B, Marrero S, Balco G, Caffee M, Goehring B, Lifton N, Nishiizumi K, Phillips F, Schaefer J, Stone J, 2016. Geological calibration of spallation production rates in the CRONUSEarth project. Quaternary Geochronology 31, 188–198.

Briner J P, Lifton N A, Miller G H, Refsnider K, Anderson R K, Finkel R, 2014. Using *in situ* cosmogenic ^{10}Be, ^{14}C, and ^{26}Al to decipher the history of polythermal ice sheets. Quaternary Geochronology 19, 4–13.

Brydsten L, 2009. Sediment dynamics in the coastal areas of Forsmark and Laxemar during an interglacial. SKB TR-09-07, Svensk Kärnbränslehantering AB.

Dunai T, 2010. Cosmogenic Nuclides: Principles, Concepts and Applications in the Earth Surface Sciences. Cambridge: Cambridge University Press.

Goodfellow B W, Lewerentz A, Stroeven A P, 2020. Petrological investigations of cosmogenic ^{14}C sampling sites at Forsmark and Uppland, 8-10-2020. SKBdoc 2016212 ver 2.0, Svensk Kärnbränslehantering AB.

Gosse J C, Phillips F M, 2001. Terrestrial in situ cosmogenic nuclides: theory and application. Quaternary Science Reviews 20, 1475–1560.

Hall A M, Ebert K, Goodfellow B W, Hättestrand C, Heyman J, Krabbendam M, Moon S, Stroeven A P, 2019. Past and future impact of glacial erosion in Forsmark and Uppland. SKB TR-19-07 Svensk Kärnbränslehantering AB.

Hedenström A, Risberg J, 2003. Shore displacement in northern Uppland during the last 6 500 calender years. SKB TR-03-17, Svensk Kärnbränslehantering AB.

Hippe K, Lifton N A, 2014. Calculating isotope ratios and nuclide concentrations for in situ cosmogenic ^{14}C Analyses. Radiocarbon 56, 1167–1174.

Ivy-Ochs S, Kober F, 2008. Surface exposure dating with cosmogenic nuclides. Quaternary Science Journal 57, 157–189.

Kim KJ, Lal D, Englert PAJ, Southon J, 2007. In situ ^{14}C depth profile of subsurface vein quartz samples from Macraes Flat New Zealand. Nuclear Instruments and Methods in Physics Research B: Beam Interactions with Materials and Atoms 259, 632–636.

Kleman J, Hättestrand M, Borgström I, Preusser F, Fabel D, 2020. The Idre marginal moraine – an anchorpoint for Middle and Late Weichselian ice sheet chronology. Quaternary Science Advances 2, 100010.

Kleman J, Stroeven A P, Lundqvist J, 2008. Patterns of Quaternary ice sheet erosion and deposition in Fennoscandia and a theoretical framework for explanation. Geomorphology 97, 73–90.

Koester A, Lifton N A, 2023. Technical note: A software framework for calculating compositionally dependent in situ ^{14}C production rates. Geochronology 5, 21–33.

Lal D, 1991. Cosmic ray labeling of erosion surfaces: in situ nuclide production rates and erosion rates. Earth and Planetary Science Letters 104, 424–439.

Lifton N, 2016. Implications of two Holocene time-dependent geomagnetic models for cosmogenic nuclide production rate scaling. Earth and Planetary Science Letters 433, 257–268.

Lifton N, Caffee M, Finkel R, Marrero S, Nishiizumi K, Phillips F M, Goehring B, Gosse J, Stone J, Schaefer J, Theriault B, 2015. *In situ* cosmogenic nuclide production rate calibration for the CRONUS-Earth project from Lake Bonneville, Utah, shoreline features. Quaternary Geochronology 26, 56–69.

Lifton N, Sato T, and Dunai T J, 2014. Scaling *in situ* cosmogenic nuclide production rates using analytical approximations to atmospheric cosmic-ray fluxes. Earth and Planetary Science Letters, 386, 149–160.

Lifton N, Wilson J, Koester A, 2023. Technical note: Studying Li-metaborate fluxes and low-temperature combustion/high-temperature extraction systematics with a new, fully automated *in situ* cosmogenic ^{14}C processing system at PRIME Lab, EGUsphere [preprint], https://doi.org/10.5194/egusphere-2023-926

Lundqvist J, 1990. The Younger Dryas event in Scandinavia. In: Lundqvist, J, Saarnisto M (eds), Termination of the Pleistocene. Geological Survey of Finland 31, 5–24.

Lupker M, Hippe K, Wacker L, Kober F, Maden C, Braucher R, Bourlès D, Romani J R V, Wieler R, 2015. Depth-dependence of the production rate of *in situ* ^{14}C in quartz from the Leymon High core, Spain. Quaternary Geochronology 28, 80–87.

Margold M, Gosse J C, Hidy A J, Woywitka R J, Young J M, Froese D, 2019. Beryllium-10 dating of the Foothills Erratics Train in Alberta, Canada, indicates detachment of the Laurentide Ice Sheet from the Rocky Mountains at ~15 ka. Quaternary Research 92, 469–482.

Marrero S M, Phillips F M, Caffee M W, Gosse J C, 2016. CRONUS-Earth cosmogenic ^{36}Cl calibration. Quaternary Geochronology 31, 199–219.

Norris S, Larasov L, Monteath A J, Gosse J C, Hidy A J, Margold M, Froese D G, 2022. Rapid retreat of the southwestern Laurentide Ice Sheet during the Bølling-Allerød interval. Geology 50, 417–421.

Phillips F M, Argento D C, Balco G, Caffee M W, Clem J, Dunai T J, Finkel R, Goehring B, Gosse J C, Hudson A M, Jull A J T, Kelly M A, Kurz M, Lal D, Lifton N, Marrero S M, Nishiizumi K, Reedy R C, Schaefer J, Stone J O H, Swanson T, Zreda M G, 2016. The CRONUS-Earth Project: A synthesis. Quaternary Geochronology 31, 119–154.

Påsse T, Daniels J, 2015. Past shore-level and sea-level displacements. Uppsala: Sveriges geologiska undersökning. (Rapporter och meddelanden 137)

Risberg J, 1999. Strandförskjutningen i nordvästra Uppland under subboreal tid. In Segerberg A (ed). Bälinge mossar: kustbor i Uppland under yngre stenålder. PhD thesis. Uppsala University, Appendix 4.

Robertsson A-M, Persson C, 1989. Biostratigraphical studies of three mires in northern Uppland, Sweden. Uppsala: Sveriges geologiska undersökning. (Serie C 821)

Schildgen T F, Phillips W M, Purves R S, 2005. Simulation of snow shielding corrections for cosmogenic nuclide surface exposure studies. Geomorphology 64, 67–85.

Schimmelpfennig I, Schaefer J M, Goehring B M, Lifton N, Putnam A E, Barrell D J, 2012. Calibration of the *in situ* cosmogenic ^{14}C production rate in New Zealand's Southern Alps. Journal of Quaternary Science 27, 671–674.

SKB, 2020. Post-closure safety for the final repository for spent nuclear fuel at Forsmark – Climate and climate-related issues, PSAR version. SKB TR-20-12, Svensk Kärnbränslehantering AB.

SKB, 2023a. Post-closure safety for SFR, the final repository for short-lived radioactive waste at Forsmark. Climate and climate-related issues, PSAR version. SKB TR-23-05, Svensk Kärnbränslehantering AB.

SKB, 2023b. Sample site photos and petrology. SKBdoc 2016213 ver 1.0, Svensk Kärnbränslehantering AB.

Small D, Clark C D, Chiverrell R C, Smedley R K, Bateman M D, 2017. Devising quality assurance procedures for assessment of legacy geochronological data relating to deglaciation of the last British-Irish Ice Sheet. Earth-Science Reviews 164, 232–250.

Stephens M B, Jansson N F, 2020. Chapter 6, Paleoproterozoic (1.9–1.8 Ga) syn-orogenic magmatism, sedimentation and mineralization in the Bergslagen lithotectonic unit, Svecokarelian orogen. In M B Stephens and J Bergman Weihed (eds). Sweden: Lithotectonic Framework, Tectonic Evolution and Mineral Resources. Geological Society of London Memoirs 50, 105–206.

Stroeven A P, Hättestrand C, Kleman J, Heyman J, Fabel D, Fredin O, Goodfellow B W, Harbor J M, Jansen J D, Olsen L, Caffee M W, Fink D, Lundqvist J, Rosqvist G C, Strömberg B, Jansson K N, 2016. Deglaciation of Fennoscandia. Quaternary Science Reviews 147, 91–12.

Strömberg B, 1989. Late Weichselian deglaciation and clay varve chronology in east-central Sweden. Uppsala: Sveriges geologiska undersökning. (Serie Ca 73)

Young N E, Schaefer J M, Goehring B, Lifton N, Schimmelpfennig I, Briner J P, 2014. West Greenland and global *in situ* ^{14}C production-rate calibrations. Journal of Quaternary Science 29, 401–406.

Arkitektkopia AB, Bromma, 2023

SKB is responsible for managing spent nuclear fuel and radioactive waste produced by the Swedish nuclear power plants such that man and the environment are protected in the near and distant future.

skb.se